P-adaptive FE-BI analysis of homogeneous, lossy regions for SAR- and far-field calculations

Matthys M. Botha* & David B. Davidson
University of Stellenbosch, South Africa, mmbotha@sun.ac.za

Abstract: This paper presents novel performance results for p-adaptive FE-BI analysis of externally excited, homogeneous, lossy regions in free space. After reviewing the theory, results are presented, leading to the conclusion that the adaptive scheme cannot reduce the solution time, but can reduce the memory requirements by 15-25%.

1 Introduction

This paper presents p-adaptive results, based upon a hybrid finite element-boundary integral (FE-BI) formulation (time-harmonic, electric field, Galerkin finite element method (FEM) using tetrahedral, curl-conforming, vector elements and hybridized with the EFIE MoM [1]). Problems of externally excited, homogeneous, lossy regions are considered, with the object of calculating average specific absorbtion rate (SAR)- and far-field values. Such problems are of great industrial interest, since problems of antenna-human interaction for establishing safety guidelines, fall into this category, which motivates the focus on SAR and far-field values. Such problems tend to be electrically large, therefore it is important to make optimal use of the available computational resources — hence p-adaptation is investigated for this class of problems, to which the FE-BI formulation is well suited. P-adaptive FE analysis uses a posteriori error indicators to selectively upgrade elemental polynomial orders. The adaptive scheme and error indicators used here, were chosen because they perform very well for antenna and waveguide problems [2].

The computational formulation is presented first, followed by an evaluation of the adaptive scheme's performance, which is the main contribution of this paper.

2 Computational formulation

This section outlines the computational formulation. The variational formulation is reviewed first, followed by descriptions of the two a posteriori error indicators and the adaptive algorithm.

2.1 Variational formulation, discretization and solution

The variational boundary value problem (VBVP), which forms the basis of the formulation, results from applying the standard Galerkin weighting procedure to the electric field, vector wave equation on the 3D domain Ω (cf. [2, 1]), yielding

$$\begin{cases} B(\mathbf{E},\mathbf{W}) = L(\mathbf{W}) \quad \forall\ \mathbf{W} \in W \\ \mathbf{E} \in W \end{cases} \tag{1}$$

$$W = \{\mathbf{a} \in H(\mathrm{curl},\Omega) \mid \hat{n} \times \mathbf{a} = 0 \text{ on } \Gamma_D\} \tag{2}$$

$$B(\mathbf{E},\mathbf{W}) = \int_\Omega \frac{1}{\mu_r} \nabla \times \mathbf{E} \cdot \nabla \times \mathbf{W}\, dV - k_0^2 \int_\Omega \epsilon_r \mathbf{E} \cdot \mathbf{W}\, dV \tag{3}$$

$$L(\mathbf{W}) = -jk_0 Z_0 \int_\Omega \mathbf{J} \cdot \mathbf{W}\, dV - \int_{\Gamma_N} \frac{1}{\mu_r} \mathbf{N} \cdot \mathbf{W}\, dS. \tag{4}$$

$\hat{n} \times \nabla \times \mathbf{E} = \mathbf{N}$ is an arbitrary, inhomogeneous Neumann boundary condition (BC) enforced on Γ_N ($\Gamma_N \subseteq \partial\Omega$). The homogeneous, Dirichlet BC $\hat{n} \times \mathbf{E} = 0$ is enforced on Γ_D through a restriction on the solution space, W (Γ_D may include parts of $\partial\Omega$ as well as surfaces internal to Ω). ($H(\mathrm{curl},\Omega)$ is the space of vector functions with finite curl on Ω.) Here, only a free space, non-local, BI, Neumann BC is considered on $S = \Gamma_N = \partial\Omega$ (based on the EFIE –

0-7803-7846-6/03/$17.00 ©2003 IEEE

see [1]), with $\Gamma_D = \emptyset$. Since only external (MoM) excitations are considered, the internal, impressed current sources are set to zero, (i.e. $\mathbf{J} = 0$ in equation (4)).

The VBVP is solved by approximating the space W by hierarchical, curl-conforming, vector basis functions of orders CT/LN or LT/QN [3], on a tetrahedral mesh consisting of N_τ elements. The outward-looking approach is used and the resulting matrix equation is solved iteratively (Conjugate Gradient Method), with a preconditioner based on incomplete LU factorization, yielding the approximate solution $\mathbf{E}_h$, to equation (1). As a consequence of the present MoM implementation only employing RWG basis functions, all BI surface basis functions must be CT/LN. Therefore, the BI boundary discretization's mesh size must be sufficiently small, since its polynomial order cannot be increased in the adaptive scheme.

2.2 A posteriori error indicators

This section presents the two error indicators. An error indicator assigns a positive real value to every element, η_i $(i = 1, .., N_\tau)$, indicating the relative magnitude of the solution error in that element, as measured in some norm, with the solution error defined as $\mathbf{e}_h = \mathbf{E} - \mathbf{E}_h$.

2.2.1 Explicit, residual-based error indicator

This type of indicator is presented in [4, 5], among others. For the formulation at hand, the elemental indicators are defined in terms of volume and face residuals, as follows [2]:

$$\eta_i = h_i^2 \|\mathbf{R}_V\|^2_{L^2(K_i)} + 0.5 \sum_{f \subset \partial K_i} h_f \|\mathbf{R}_f\|^2_{L^2(f)}, \tag{5}$$

$$h_i = \operatorname{diam}(K_i) \tag{6}$$

$$h_f = \begin{cases} \max\left\{\operatorname{diam}(K^{(1)}), \operatorname{diam}(K^{(2)})\right\} & \text{internal face} \\ \operatorname{diam}(K^{(1)}) & \text{boundary face} \end{cases} \tag{7}$$

$$\mathbf{R}_V = -\nabla \times \frac{1}{\mu_r} \nabla \times \mathbf{E}_h + k_0^2 \epsilon_r \mathbf{E}_h - j k_0 Z_0 \mathbf{J} \quad \text{in } K_i;\ i = 1, ..., N_\tau \tag{8}$$

$$\mathbf{R}_f = \begin{cases} \hat{n}^{(12)} \times \left[\dfrac{1}{\mu_r^{(1)}} \nabla \times \mathbf{E}_h^{(1)} - \dfrac{1}{\mu_r^{(2)}} \nabla \times \mathbf{E}_h^{(2)} \right] & \text{on } \ f \not\subseteq (\Gamma_D \cup S) \\ 0 & \text{on } \ f \subseteq (\Gamma_D \cup S) \end{cases} \tag{9}$$

The superscripts (1) and (2) designate association with the first and second elements sharing a face. The normal vector $\hat{n}^{(12)}$ points from the first element to the second element, normal to their shared face. Note that the volume and face residuals will all be equal to zero if $\mathbf{E}_h$ is the exact solution. Observe that, theoretically, the face residuals on S must be defined as the discontinuity in the tangential magnetic field intensity of the approximate solution. This calculation is not supported in the current implementation, therefore, the face residuals on S are assumed to be zero, which is consistent with the fixed (assume "perfect") nature of the discretization on S (remarked upon in Section 2.1).

2.2.2 Implicit, residual-based error indicator

This type of indicator is presented in [4], among many others. Elemental, Neumann BC, VBVPs are solved in order to obtain an approximation of the error field in terms of higher order basis functions. The VBVP on an elemental volume K, for the formulation at hand, is defined as follows [2]:

$$\begin{cases} B_K(\mathbf{e}_h, \mathbf{W}) = L_K(\mathbf{W}) - B_K(\mathbf{E}_h, \mathbf{W}) \\ -\dfrac{1}{2} \displaystyle\sum_{f \subseteq \partial K \setminus (\Gamma_D \cup S)} \int_f \left(\hat{n} \times \left[\frac{1}{\mu_r^{(1)}} \nabla \times \mathbf{E}_h^{(1)} + \frac{1}{\mu_r^{(2)}} \nabla \times \mathbf{E}_h^{(2)} \right] \right) \cdot \mathbf{W} \, dS \\ \forall\ \mathbf{W} \in W_K\ ; \quad \mathbf{e}_h \in W_K \end{cases} \tag{10}$$

$$W_K = \{\mathbf{a} \in H(\text{curl}, K) \mid \hat{n} \times \mathbf{a} = 0 \text{ on } \partial K \cap (\Gamma_D \cup S)\} \tag{11}$$

$$B_K(\mathbf{E}, \mathbf{W}) = \int_K \frac{1}{\mu_r} \nabla \times \mathbf{E} \cdot \nabla \times \mathbf{W}\, dV - k_0^2 \int_K \epsilon_r \mathbf{E} \cdot \mathbf{W}\, dV \tag{12}$$

$$L_K(\mathbf{W}) = -jk_0 Z_0 \int_K \mathbf{J} \cdot \mathbf{W}\, dV. \tag{13}$$

Again, it is assumed that the tangential components of the error field is equal to zero on S, for the same reason as stated in Section 2.2.1. Equation (10) is solved by approximating W_K with the elemental LT/QN space. Together, the elemental solutions yield an approximate global solution $\tilde{\mathbf{e}}_h$. The elemental error indicators are obtained by measuring $\tilde{\mathbf{e}}_h$ on an element-wise basis with a suitable norm. Based on the intended application, define the average SAR-norm as follows (derived from the definition of SAR [6]):

$$\|\mathbf{a}\|_{\text{SAR}(\Omega)} \equiv \frac{1}{2\,\text{Volume}(\Omega)} \int_\Omega \frac{\sigma}{\rho} \mathbf{a} \cdot \mathbf{a}^*\, dV, \tag{14}$$

yielding the error indicators

$$\eta_i = \|\tilde{\mathbf{e}}_h\|_{\text{SAR}(K_i)}. \tag{15}$$

2.3 The p-adaptive algorithm

The adaptive algorithm consists of a single solve-refine-re-solve cycle. Based on an initial all-CT/LN solution, error indicators are calculated (using either type) and a specified percentage of elements, with the largest error indicator values, are upgraded to LT/QN. The problem is re-solved to obtain the final result.

3 Results

Lossy sphere problems are considered. For these problems the average SAR- and far-field values generally converge at a discretization level of $\frac{\lambda}{3.6}$ in the LT/QN case, but not in the CT/LN case. The presented results (at this discretization level) show convergence relative to all-LT/QN solutions of average SAR and far-field back scattering, as functions of solution time and memory usage, as the upgrade percentage is increased. Two problems are considered — they are spheres with $\epsilon_r = 40 - j10$ and radii $r = 0.5\lambda$ and $r = 2.0\lambda$. The spheres are modelled with a free space layer on the outside, of thickness $\frac{\lambda_0}{32}$, with outside surface discretization $\frac{\lambda_0}{20}$. Figure 1 presents results for the $r = 0.5\lambda$ problem. The sphere is excited with an E_θ-polarized plane wave, incident from $(\phi, \theta) = (0°, 180°)$. Figure 2 presents results for the $r = 2.0\lambda$ problem. The sphere is excited with a dipole, centered on the negative z-axis and parallel to the x-axis, located $\frac{\lambda_0}{32}$ away from the FEM boundary (i.e. $\frac{\lambda_0}{16}$ away from the lossy region).

It was found that these results cannot be improved upon by keeping to CT/LN elements and uniformly refining the mesh. These results indicate that solution time cannot be reduced, but that memory requirements can be reduced by $15 - 25\%$. The explicit indicator is always superior to the implicit one, which could possibly be attributed to the stronger theoretical foundation of the former [2]. The type of external excitation does not play a significant role in the effectiveness of the error indicators.

4 Conclusion

The presented p-adaptive scheme's performance was evaluated in terms of integral quantities (SAR and far-field values) for externally excited, lossy regions. In this setting, it was found that the two error indicators considered are useful, but not highly effective, with their use only leading to a reduction in memory requirements. In [2] it is shown that they perform very well when strong field variations are present (eg. at sharp PEC edges where the electric field becomes singular), but that they are less effective on homogeneous domains — which

correlates well with the findings presented here. An error indicator which also takes the error in the solution's divergence into account (the charge buildup error), might possibly lead to a meaningful improvement upon the adaptive results presented here. The authors gratefully acknowledge the support of Electromagnetic Software & Systems (Dr F.J.C. Meyer).

References

[1] J. Jin, *The Finite Element Method in Electromagnetics*. New York: John Wiley and Sons, 2nd ed., 2002.

[2] M. M. Botha, *Efficient finite element electromagnetic analysis of antennas and microwave devices: the FE-BI-FMM formulation and a posteriori error estimation for p adaptive analysis*. PhD thesis, University of Stellenbosch, Stellenbosch, South Africa, 2002.

[3] J. S. Savage, "Comparing high order vector basis functions," in *Proceedings of the 14th Annual Review of Progress in Applied Computational Electromagnetics*, pp. 742–749, March 1998. Monterey, CA.

[4] M. Ainsworth and J. T. Oden, "A posteriori error estimation in finite element analysis," *Computer Meth. in Appl. Mech. and Eng*, vol. 142, pp. 1–88, 1997.

[5] K. Eriksson, D. Estep, P. Hansbo, and C. Johnson, "Introduction to adaptive methods for differential equations," *Acta Numerica*, pp. 105–158, 1995.

[6] A. Ishimaru, *Electromagnetic Wave Propagation, Radiation, and Scattering*. Englewood Cliffs, New Jersey: Prentice-Hall, 1991.

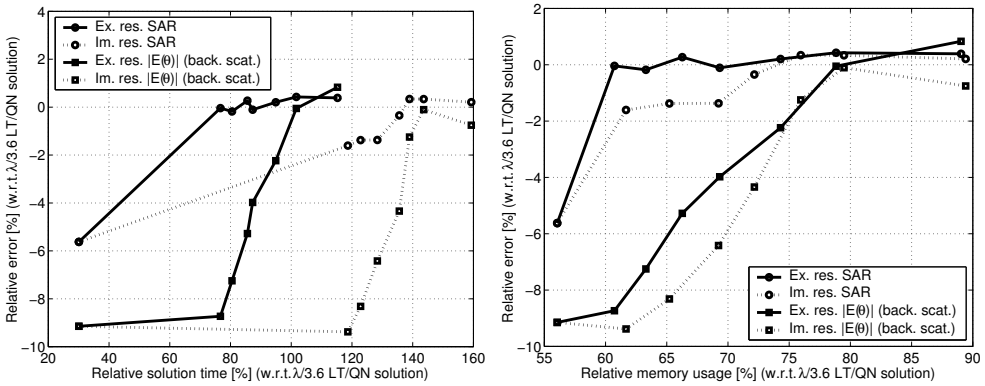

Figure 1: Comparison of convergence of observable quantities w.r.t. solution time and memory usage, as the upgrade percentage is increased for the $r = 0.5\lambda$ sphere problem with plane wave excitation. LT/QN memory usage = 5.61184 MByte. LT/QN DOFs = 4620.

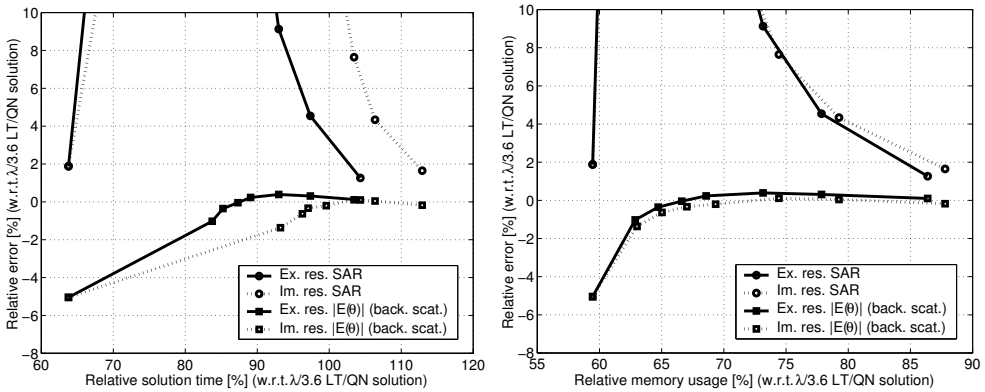

Figure 2: Comparison of convergence of observable quantities w.r.t. solution time and memory usage, as the upgrade percentage is increased for the $r = 2.0\lambda$ sphere problem with dipole excitation. LT/QN memory usage = 213.27109 MByte. LT/QN DOFs = 153908.